*Annual Review of Fluid Mechanics*

# Numerical Models of Surface Tension

Stéphane Popinet

Institut Jean le Rond d'Alembert, UMR 7190, Université Pierre et Marie Curie Paris 06, Centre National de la Recherche Scientifique, Sorbonne Universités, F-75005 Paris, France;
email: stephane.popinet@upmc.fr

Annu. Rev. Fluid Mech. 2018. 50:49–75

First published as a Review in Advance on August 7, 2017

The *Annual Review of Fluid Mechanics* is online at fluid.annualreviews.org

https://doi.org/10.1146/annurev-fluid-122316-045034





## Keywords

well-balanced, Eulerian, level set, volume of fluid, curvature, height function, implicit, stability

## Abstract

Numerical models of surface tension play an increasingly important role in our capacity to understand and predict a wide range of multiphase flow problems. The accuracy and robustness of these models have improved markedly in the past 20 years, so that they are now applicable to complex, three-dimensional configurations of great theoretical and practical interest. In this review, I attempt to summarize the most significant recent developments in Eulerian surface tension models, with an emphasis on well-balanced estimation, curvature estimation, stability, and implicit time stepping, as well as test cases and applications. The advantages and limitations of various models are discussed, with a focus on common features rather than differences. Several avenues for further progress are suggested.

## 1. INTRODUCTION

Natural philosophers have noticed the effects of surface tension since the time of Aristotle, who recorded that flat pieces of iron or lead could float on the surface of water [see Aristotle 1922 (350 BC)]. A solid understanding of the phenomenon had to wait until 1805, when Young and Laplace independently published comprehensive theories of capillarity inspired by the speculations of their predecessors [including Newton, von Segner, and Monge; for a history of surface tension, the reader is referred to the article by Maxwell (1889) and the commentary on it by Pomeau (2013)]. Besides its connection to modern understanding of the molecular nature of matter, surface tension is closely associated with major developments in differential geometry [by Clairaut, Monge, and, especially, Gauss (1830), who formalized the analysis of minimal surfaces].

The coupling between volumetric fields and the geometry of surfaces is, indeed, at the heart of theoretical and numerical models of surface tension. From an analytical perspective, taking into account the (nonlinear) boundary conditions imposed on a surface that is itself part of the unknown solution presents formidable difficulties; analytical solutions are thus usually restricted to small surface deformations or static configurations (many of which were already obtained by Young, Laplace, Gauss, and, later, Plateau).

A natural way to obtain numerical approximations for surface tension is to use boundary-conforming discretizations, in which a Lagrangian description of volumetric fields is constructed so that the boundaries of volume elements coincide with the moving interface or free surface. Imposing the boundary or jump conditions given by surface tension is then relatively straightforward (see, e.g., Fyfe et al. 1988 for an early example). The price to pay for this conceptual simplicity is the geometric complexity of Lagrangian methods, where the mesh needs to adapt to the underlying deformation of space.

Due to the necessity of dealing with very large deformations, Eulerian field descriptions are a natural choice for fluid mechanics (in contrast to solid mechanics). They can be coupled with either a Lagrangian or an Eulerian representation of the interface. Lagrangian interface representation methods include the pioneering marker-and-cell method of Harlow & Welch (1965), the immersed-boundary method of Peskin (1972), the front-tracking method of Tryggvason and collaborators (Unverdi & Tryggvason 1992, Tryggvason et al. 2001), and the marker technique of Popinet & Zaleski (1999). Eulerian interface representations include the volume-of-fluid (VOF) (Scardovelli & Zaleski 1999), level-set (Sussman et al. 1994, Sethian & Smereka 2003), and phase-field methods (Anderson et al. 1998).

Surface (interface) and volume (fields) representations are then coupled through either (*a*) interface kinematics, i.e., the transport by the Eulerian velocity field of the Lagrangian or Eulerian interface description, or (*b*) interfacial dynamics, i.e., changes in material properties (density and viscosity) and boundary or jump conditions associated with the interface. For Lagrangian interface representations, transport is simple and accurate; however, difficulties arise for large deformations and especially for breakup and coalescence. Eulerian interface descriptions can deal transparently with changes of topology but lead to more complex transport schemes. The solution to this kinematic problem has seen major progress in the past 25 years, with the development of higher-order geometric VOF methods that guarantee nondiffusive, sharp interface motion (Gueyffier et al. 1999); conservative level-set methods (Desjardins et al. 2008, Xiao et al. 2011); and coupled VOF–level-set methods (Sussman & Puckett 2000).

The situation for interfacial dynamics, and surface tension in particular, is more complex, and a wide range of methods or combinations of methods is available, often with limited information on the relative merits of each method. The aim of this review is to highlight the most significant developments in Eulerian surface tension models in the past 20 years, with a specific emphasis on

well-balanced estimation, curvature estimation, stability, and implicit time stepping, as well as test cases and applications.

## 2. SURFACE TENSION FORMULATIONS

Let us consider the Navier–Stokes equations for incompressible flow with surface tension:

$$\begin{aligned} \partial_t \rho + \mathbf{u} \cdot \nabla \rho &= 0, \\ \rho \left(\partial_t \mathbf{u} + \mathbf{u} \cdot \nabla \mathbf{u}\right) &= \nabla \cdot \left[\mu \left(\nabla \mathbf{u} + \nabla^T \mathbf{u}\right)\right] - \nabla p + \mathbf{f}_\sigma, \\ \nabla \cdot \mathbf{u} &= 0, \end{aligned}$$

where $\rho$ and $\mu$ are the variable density and viscosity, respectively; $\mathbf{u}$ is the velocity; $p$ is the pressure; and $\mathbf{f}_\sigma$ is the surface tension force per unit volume. The equation of continuity requires the solution of the kinematic problem mentioned in Section 1, i.e., (nondiffusive) interfacial transport. The assumption of incompressibility means that pressure loses its thermodynamic definition and reduces to the constraint necessary to impose a divergence-free velocity. This can be used to rearrange body forces, as is done below.

### 2.1. Integral Formulation

Perhaps the most natural way to derive an expression for $\mathbf{f}_\sigma$ is to consider the forces acting on a two-dimensional curve under tension, as was done by Young (1805). In the case of interfaces between fluids (which is different for thin membranes), two-dimensional tension is simply a force per unit length tangential to the curve, which can be expressed as $\sigma \mathbf{t}$, where $\mathbf{t}$ is the unit tangent vector and $\sigma$ is the surface tension coefficient. If we now consider an elementary volume $\Omega$, intersected by the curve in two points $A$ and $B$, the total tension force acting on $\Omega$ is

$$\int_\Omega \mathbf{f}_\sigma = \oint_A^B \sigma \, \mathrm{d}\mathbf{t} = \sigma_B \mathbf{t}_B - \sigma_A \mathbf{t}_A, \qquad 1.$$

where the second integral is along the interface and where $\sigma_A$ and $\sigma_B$ are the (possibly different) surface tension coefficients at $A$ and $B$. The resultant of surface tension forces on the control volume thus reduces to the sum of tensions at the entry and exit points of the interface.

From a numerical perspective, this formulation has several advantages. First, it only involves low-order derivatives of the geometry, which should lead to accurate numerical estimates. Second, in a manner similar to flux-based integration of the divergence operator in finite-volume schemes, the contributions of surface tension forces to neighboring control volumes cancel out exactly (the directions of the unit tangent vectors in Equation 1 are simply reversed). This can be interpreted as the divergence of a surface stress and is related to the continuum surface stress formulation of Gueyffier et al. (1999). This ensures exact local and global momentum conservation for surface tension. In particular, the net force exerted on the fluid by a closed interface is exactly zero. This is not the case for the volumetric force formulations discussed in Section 2.2.

Popinet & Zaleski (1999) used this formulation in combination with a Lagrangian representation of the interface and obtained very accurate results (compared to methods available at the time), in particular for Laplace balance and capillary waves. This required a consistent finite-volume discretization of the pressure gradient, taking into account the pressure jump across the interface at the intersection points.

In the context of front-tracking techniques, the generalization of Equation 1 to three dimensions (Weatherburn 1927) has been used by Tryggvason et al. (2001) to define a globally conservative interfacial force. However, this has not been combined with the corresponding finite-volume

integration on the Eulerian grid (instead, the surface force is spread over the Eulerian grid using a smoothing kernel), so that the final scheme shares some of the properties of the volumetric force formulations in the next section.

## 2.2. Volumetric Formulation

Using the first Frenet formula for parametric curves $\mathrm{d}\mathbf{t} = \kappa \mathbf{n} \mathrm{d}s$, where $\kappa$ is the curvature, $\mathbf{n}$ is the unit normal, and $s$ is the curvilinear coordinate, gives (for a constant surface tension coefficient)

$$\int_\Omega \mathbf{f}_\sigma = \oint_A^B \sigma \ \mathrm{d}\mathbf{t} = \oint_A^B \sigma\kappa\mathbf{n} \ \mathrm{d}s = \int_\Omega \sigma\kappa\mathbf{n}\delta_s,$$

where $\delta_s$ is a surface Dirac $\delta$-function that is nonzero only on the interface (see Tryggvason et al. 2011, appendix B, for a detailed derivation). Note that, in the case of variable surface tension, tangential (Marangoni) stresses need to be added to this formulation (whereas they are naturally taken into account in the integral formulation).

Volumetric formulations are based on a numerical approximation of the surface Dirac function, which allows a direct evaluation of the volumetric force $\sigma\kappa\mathbf{n}\delta_s$. This approach can be traced back to the original immersed boundary method of Peskin (1972), although this link is not always acknowledged in subsequent articles. Most methods belong to this category regardless of the way the interface is represented. The idea is to use the relation

$$\sigma\kappa\delta_s\mathbf{n} = \sigma\kappa\nabla H\,(\mathbf{x} - \mathbf{x}_s),$$

where $H$ is the Heaviside function and $\mathbf{x}_s$ is the position of the interface. The next step is to choose a suitable numerical approximation $H_\epsilon$ of the Heaviside function, which will typically depend on a (small) parameter $\epsilon$ such that

$$\lim_{\epsilon\to 0} H_\epsilon = H.$$

The small parameter $\epsilon$ is a length scale related to the characteristic thickness of the interface. Depending on this choice, which is linked to the type of interface representation, different methods can be constructed.

In the continuum surface force (CSF) method of Brackbill et al. (1992), the interface is represented through the volume fraction field $c$, and one simply sets $H_\epsilon = c$ with $\epsilon = \Delta$ the mesh size. In the original CSF paper (Brackbill et al. 1992), $c$ is replaced with a filtered or smoothed version $\tilde{c}$, which increases the characteristic interface thickness $\epsilon$. This is not necessary at this stage, however, as it mostly relates to a different issue, the estimation of interfacial curvature, which is addressed in Section 4.

The original method of Peskin (1972) is designed for elastic membranes, rather than interfaces, and relies on an explicit Lagrangian description of the membrane. Unverdi & Tryggvason (1992) extended this approach to interfaces using an indicator function reconstructed from the Lagrangian description as an approximation of the Heaviside function. Sussman et al. (1994) proposed to use a representation of the interface as the zero contour of a level-set function $\phi$. The Heaviside function is then approximated as a smooth function such as

$$H_\epsilon(\mathbf{x} - \mathbf{x}_s) = H_\epsilon(\phi(\mathbf{x})) = \begin{cases} 0 & \text{if } \phi(\mathbf{x}) < -\epsilon \\ 1 & \text{if } \phi(\mathbf{x}) > \epsilon \\ \dfrac{1 + \phi/\epsilon + \sin(\pi\phi/\epsilon)/\pi}{2} & \text{otherwise} \end{cases}. \qquad 2.$$

In the common case, where $\phi$ is chosen to be the signed distance to the interface, $\epsilon$ is the characteristic interface thickness (see Engquist et al. 2005 for a detailed discussion).

Another type of surface tension discretization usually associated with level-set interface representations is the ghost fluid method (GFM) (Fedkiw et al. 1999, Kang et al. 2000). Although this may not be obvious at first, this method can also be recast as a volumetric force formulation. Rather than including the surface tension as a surface force, Fedkiw et al. (1999) proposed to directly include the corresponding jump condition in the discretization of the pressure gradient operator. This is essentially the immersed interface approach of LeVeque & Li (1994), itself a formalization of Peskin's immersed boundary method.

Let us consider a simple second-order discretization of a one-dimensional pressure gradient operator, which can be written

$$(\nabla p)_{i-1/2} = \frac{p_i - p_{i-1}}{\Delta},$$

where $\Delta$ is the grid spacing. The GFM proposes to modify this operator locally in order to take into account the pressure jump induced by surface tension. This leads to the following scheme:

$$(\nabla^\star p)_{i-1/2} = \frac{1}{\Delta}\begin{cases} p_i^- - p_{i-1} & \text{if the interface is in } [x_{i-1} : x_i] \\ p_i - p_{i-1} & \text{otherwise} \end{cases},$$

with the ghost fluid value $p_i^- = p_i \pm (\sigma\kappa)_{i-1/2}$, where the sign of the jump depends on the orientation of the interface. This can be rewritten as

$$(\nabla^\star p)_{i-1/2} = (\nabla p)_{i-1/2} - (\sigma\kappa\delta)_{i-1/2},$$

with

$$\delta_{i-1/2} = \begin{cases} \pm 1/\Delta & \text{if the interface is in } [x_{i-1} : x_i] \\ 0 & \text{otherwise} \end{cases}. \qquad 3.$$

Note that $\delta_{i-1/2}$ is indeed a consistent approximation of a Dirac delta function. The corresponding approximation of the Heaviside function is

$$H_i = \begin{cases} 1 & \text{if } x_i \text{ is inside the interface} \\ 0 & \text{otherwise} \end{cases}, \qquad 4.$$

and $\delta_{i-1/2}$ in Equation 3 is

$$\delta_{i-1/2} = (\nabla H)_{i-1/2} = \frac{H_i - H_{i-1}}{\Delta}.$$

The GFM is indeed naturally suited to a level-set representation of the interface because the inside the interface condition in Equation 4 is then $\phi_i > 0$. Note, however, that it is also applicable to a VOF representation of the interface. The standard CSF approximation of the Dirac delta,

$$\delta_{i-1/2} = (\nabla c)_{i-1/2},$$

can simply be replaced with $\delta_{i-1/2} = (\nabla H)_{i-1/2}$, where $H$ is the equivalent of the GFM approximation (Equation 4):

$$H_i = \begin{cases} 1 & \text{if } c_i > 0.5 \\ 0 & \text{otherwise} \end{cases}.$$

The CSF method (typically combined with a VOF interface representation), the smoothed Heaviside method (typically combined with level set or front tracking), and the GFM method (typically combined with level set) can all be summarized as

$$\sigma\kappa\delta_s \mathbf{n} = \sigma\kappa\nabla H.$$

The different approximations for $H$ are summarized in **Table 1**.

**Table 1 Approximations of the interface Heaviside function for different volumetric methods**

| Method | Heaviside function $H$ |
|---|---|
| CSF (VOF) | $c$ |
| Smooth (level set/front tracking) | $\begin{cases} 0 & \text{if } \phi < -\epsilon \\ 1 & \text{if } \phi > \epsilon \\ [1 + \phi/\epsilon + \sin(\pi\phi/\epsilon)/\pi]/2 & \text{otherwise} \end{cases}$ |
| GFM (level set/VOF) | $\begin{cases} 1 & \text{if } \phi > 0 \text{ (level set) or } c > 0.5 \text{ (VOF)} \\ 0 & \text{otherwise} \end{cases}$ |

Abbreviations: CSF, continuum surface force; GFM, ghost fluid method; VOF, volume of fluid.

The corresponding graphs for $H$ and $\delta$ (normalized by $\epsilon$) are represented in **Figure 1**. The fact that the approximation of the Heaviside function for the GFM looks exact has led to the claim that the GFM leads to a sharp interface representation, in contrast with the other methods. It is clear, however, that the approximation of the Dirac function is not significantly sharper for the GFM than for the other methods. In fact, all methods lead to a characteristic interface thickness of order $\epsilon = \Delta$. This is obvious for the Dirac approximations but is also true for the sharp Heaviside approximation of the GFM method because this approximation is insensitive to a shift of $\pm\epsilon/2$ of the actual position of the interface.

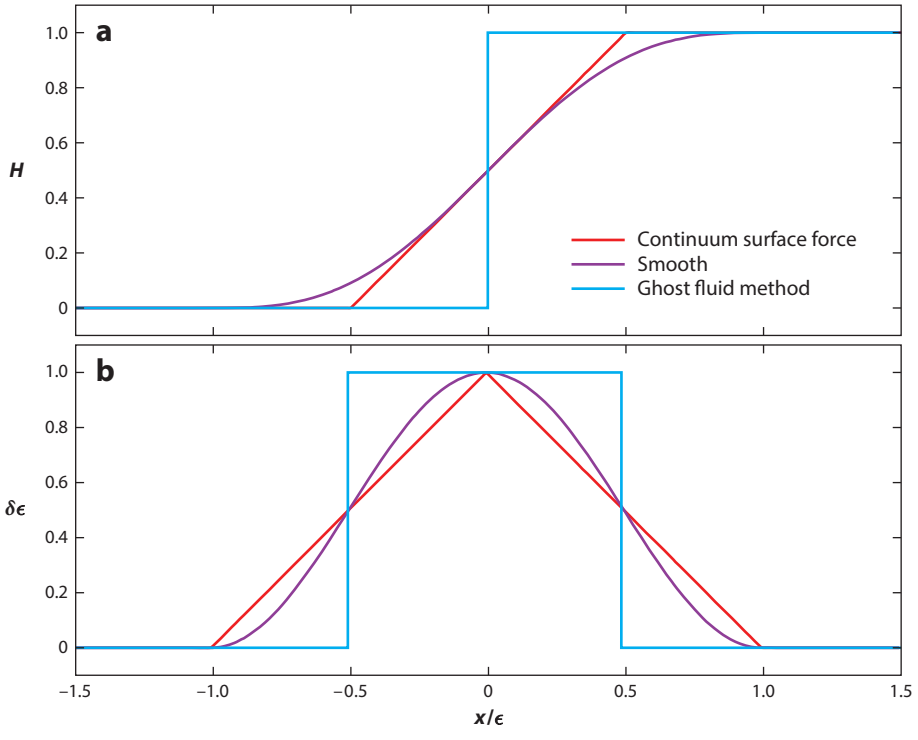


**Figure 1**

Approximations of the (*a*) interface Heaviside and (*b*) (normalized) Dirac functions for different volumetric methods.

## 3. WELL-BALANCED METHODS

A classic and nontrivial problem when designing numerical schemes for partial differential equations is ensuring that specific equilibrium solutions of the (continuous) equations are recovered by the (discrete) numerical scheme. This problem arises for a wide range of equations and applications: hyperbolic systems of conservation laws with source terms (LeVeque 1998), hydrostatic balance in $\sigma$-coordinate ocean or atmosphere models (Mesinger 1982), the topographic source term in shallow-water equations (Audusse et al. 2004), and more. Numerical schemes that recover these equilibrium solutions are often called well-balanced methods.

In the case of surface tension, setting $\mathbf{u} = 0$ in the Navier–Stokes equations, we get the equilibrium condition

$$-\nabla p + \sigma\kappa\mathbf{n}\delta_s = 0,$$

which is verified for

$$\begin{aligned}[p] &= \sigma\kappa,\\ \kappa &= \text{constant},\end{aligned}$$

where $[p]$ is the jump of the pressure across the (spherical) interface. This is the well-known Laplace's relation between pressure and surface tension in a drop in equilibrium. If we assume that each of the (nonzero) terms in the Navier–Stokes equations is approximated with second-order accuracy, the leading-order discrete equilibrium condition can be written

$$\nabla p + C_p\Delta^2 = \sigma\kappa\mathbf{n}\delta_s + C_\sigma\Delta^2,$$

where $C_p$ and $C_\sigma$ are scheme- and solution-dependent factors that control the pressure gradient and surface tension errors, respectively. If special care is not taken, these errors have no reason to cancel, and the best that one can hope for is that the equilibrium condition is verified to within the accuracy of the scheme, i.e., asymptotically to within $O(\Delta^2)$. Although this may be acceptable for some applications, for example, when surface tension is not the dominant force or when the interface is far from this equilibrium solution, in practice, two-phase interfacial flows often include drops or bubbles close to Laplace's equilibrium.

For many years, numerical methods were not able to recover this simple equilibrium solution, and the resulting quasistationary velocity pattern became known as spurious or parasitic currents, of varying intensity depending on the method. Interestingly, the volumetric force formulation leads to a very simple condition for discrete equilibrium, as first pointed out by Renardy & Renardy (2002). Indeed, we have the (exact) relation

$$-\nabla p + \sigma\kappa\mathbf{n}\delta_s = -\nabla p + \sigma\kappa\nabla H = 0,$$

which, in the case of constant $\sigma$ and $\kappa$, can be approximated as

$$-\nabla^\star(p - \sigma\kappa H) = 0,$$

where $\nabla^\star$ is a numerical approximation of the gradient (assumed to be a discrete linear operator). The exact discrete numerical solution, which guarantees exact balance between surface tension and pressure in the case of constant $\kappa$, is then simply

$$p = \sigma\kappa H + \text{constant}, \qquad 5.$$

where $H$ is one of the approximations in **Table 1**.

For a staggered, markers-and-cell (MAC) discretization, where velocity components are stored at midpoints, and pressure at the centers of a regular Cartesian grid, a simple well-balanced

scheme is

$$-\frac{p_{i+1}-p_i}{\Delta}+(\sigma\kappa)_{i+1/2}\frac{H_{i+1}-H_i}{\Delta}. \qquad 6.$$

Unfortunately, this was not the scheme adopted by Brackbill et al. (1992) in the original CSF article (for which $H = \tilde{c}$). They instead chose to compute the midpoint surface tension force as the average of cell-centered values. This means that different operators are used to compute the gradient of the pressure (at midpoints) and volume fraction (at centers), thus breaking the well-balanced property. The motivation for this choice was probably related to the desire to reuse the normal components also used to compute $\kappa = \nabla \cdot \mathbf{n}$ at cell centers.

Thus, one explanation for the relative confusion around the issue of spurious currents is linked to the contradictory requirements of a well-balanced formulation and accurate curvature estimation. A well-balanced formulation requires that the gradient of a (usually) smooth function (the pressure) be estimated using the same discrete operator as that used to estimate the gradient of a discontinuous function (the Heaviside approximation/volume fraction). It is also well known that such a gradient estimate will lead to a poor approximation of $\mathbf{n}\delta_s$ and an even poorer estimate of the curvature $\kappa = \nabla \cdot \mathbf{n}$. However, when looking for a better estimate of $\kappa$, one may be tempted to also use the better estimate of $\mathbf{n}\delta_s$ associated with it; unfortunately, this will break the well-balanced property. This is what happened in the original CSF formulation and many other early implementations.

It is thus necessary to decouple the estimate of $\mathbf{n}\delta_s$ and the estimate of $\kappa$. Note that this is what happens naturally for level-set methods. In these methods, the normal is estimated as $\mathbf{n} = \nabla\phi$ and the curvature as $\kappa = \nabla \cdot \mathbf{n}$; however, $\mathbf{n}\delta_s$ is estimated as $\nabla H$, where $H$ is computed using either a smooth function or the GFM (see **Table 1**).

Well-balanced estimation, as applied to surface tension, can (and should) be applied to any system for which a source term can be balanced by the pressure gradient. If this source term can be expressed as the gradient of a potential, a consistent discretization of the pressure and potential gradients will lead to a well-balanced scheme.

If we assume that a body force can be expressed as the gradient of a potential $\phi$ times a material property $f$, we have

$$-\nabla p + f\nabla\phi = -\nabla p + \nabla(f\phi) - \phi\nabla f = -\nabla p' - \phi\nabla f,$$

with $p' = p - f\phi$. If we now assume that the material property jumps from a constant value $f_0$ to a constant value $f_1$ across the interface, we have

$$f(H) = (f_0 - f_1)H + f_1 = [f]H + f_1,$$

where $H$ is the Heaviside function associated with the interface. This gives

$$-\nabla p + f\nabla\phi = -\nabla p' - [f]\phi\nabla H = -\nabla p' - [f]\phi\mathbf{n}\delta_s. \qquad 7.$$

The body force can thus be replaced by an interfacial force equal to the potential times the jump of material properties across the interface. Surface tension itself can be reformulated using this general relation as

$$-\nabla p - \sigma H \nabla\kappa = -\nabla p' + \sigma\kappa\mathbf{n}\delta_s, \qquad 8.$$

with $p = p' - \sigma\kappa H$ (using $\phi = \kappa$ and $f = -\sigma H$, as in Equation 7). This has the advantage of giving a naturally balanced scheme for a constant curvature without any constraint on the choice of the discrete gradient operators (aside from $\nabla$ constant $= 0$) (see Ghidaglia 2016 for a detailed derivation).

Similarly, the acceleration of gravity can be reformulated as

$$-\nabla p + \rho \mathbf{g} = -\nabla p' - [\rho]\mathbf{g} \cdot \mathbf{x}\mathbf{n}\delta_s,$$

with $p' = p - \rho \mathbf{g} \cdot \mathbf{x}$ (using $\phi = \mathbf{g} \cdot \mathbf{x}$ and $f = \rho$, as in Equation 7). The hydrostatic pressure is thus subtracted analytically, which is advantageous for ensuring exact hydrostatic balance across the interface and also simplifies boundary conditions for open domains (see, e.g., Wroniszewski et al. 2014 for an application to breaking waves).

More complex models can also be simplified using the relation in Equation 7. For example, Mahady et al. (2016) proposed to discretize the disjoining pressure induced by a potential of the form $\phi = (b^\star/y)^m$, where $y$ is the distance to the substrate, as

$$-\nabla p + K\nabla\phi = -\nabla p' - \phi[K]\mathbf{n}\delta_s,$$

which avoids dealing with the divergence of the potential close to the substrate (this divergence is balanced analytically by the corresponding divergence of the pressure $p$).



## 4. CURVATURE ESTIMATION

The accurate estimation of interface curvature is, of course, central to the performance of volumetric surface tension force models (for integral formulations, only the interface normal is required). Although the details depend on the particular technique used for interface representation, one can essentially distinguish between two classes of methods: (*a*) direct derivation from the implicit representation of the interface and (*b*) discrete differential geometry operators applied to an explicit description of the location of the interface (provided directly by the interface tracking representation or reconstructed from an implicit description of the interface).

### 4.1. Level-Set Methods

The first class of methods is the primary argument in favor of level-set interface representations. In the ideal case, where the level-set function $\phi$ is the signed distance to the interface, the curvature is simply obtained using the relations

$$\mathbf{n} = \nabla\phi \quad \text{and} \quad \kappa = \nabla \cdot \mathbf{n}. \tag{9.}$$

The level-set function $\phi$ is smooth, and discrete schemes can be easily constructed to estimate both $\mathbf{n}$ and $\kappa$ to any order of accuracy. This is the approach adopted in early articles that used the level-set method to represent interfaces and surface tension (e.g., Sussman et al. 1994). Although useful schemes can be obtained with this approach, it has an important limitation that is evident when considering the well-balanced property of the previous section. Let us consider the simple well-balanced discretization

$$-\frac{p_{i+1} - p_i}{\Delta} + (\sigma\kappa)_{i+1/2}\frac{H(\phi_{i+1}) - H(\phi_i)}{\Delta}, \tag{10.}$$

where $H$ is a suitable approximation of the Heaviside function (e.g., Equation 2 or the GFM approximation in **Table 1**). A simple estimate of the curvature is

$$\kappa_{i+1/2} = [\nabla \cdot (\nabla\phi)]_{i+1/2}, \tag{11.}$$

where the divergence and gradient operators are suitable discrete approximations. To recover Laplace's equilibrium relation (Equation 5), the estimate of the curvature needs to be constant for a spherical droplet. Note, however, that the relations in Equation 9, as well as their discretization (Equation 11), define a curvature that is everywhere in the domain, not just on the interface ($\phi = 0$).

The curvature given by Equation 9 is indeed the curvature of the local contour rather than that on the interface. In the case of a spherical interface, Equation 11 will thus return an estimate of the curvature that will not be constant, and Laplace's equilibrium will not be guaranteed. The deviation from the equilibrium solution will be controlled by the distance between the interface and the points where the curvature is estimated (i.e., at $i + 1/2$) times the value at these locations of the gradient of the Heaviside function. This distance obviously scales like the thickness of the interface (i.e., essentially the grid size) and will thus tend toward zero with spatial resolution, which makes the method consistent but not well balanced. This limitation of naive level-set methods has been recognized by, for example, Sussman & Ohta (2009), who advocated the use of a height-function curvature calculation (described below), rather than the relations in Equation 9, even in the case of a level-set description of the interface.

A closely related issue is the explanation of the improved performance of the GFM relative to the classical smoothed Heaviside level-set formulation. In the initial article by Kang et al. (2000), the decrease in spurious currents observed with the GFM is attributed to the sharper surface tension representation provided by the GFM, a conclusion that was contested in a later article by Francois et al. (2006) in connection with their sharp surface force (SSF) model (this model is actually identical to the Dirac formulation of the GFM; see Equation 3). The improvement is not due to the difference in Dirac approximations summarized in **Table 1**, but rather to the interpolation formula proposed by Kang et al. (2000) to estimate the pressure jump (i.e., the curvature) at the location of the interface [based on earlier work by Fedkiw et al. (1999)]:

$$\kappa_{i+1/2} = \frac{\kappa_i|\phi_{i+1}| + \kappa_{i+1}|\phi_i|}{|\phi_i| + |\phi_{i+1}|},$$

i.e., a distance-weighted average of the cell-centered values of the curvature, which are computed using Equation 9. In the case of a spherical interface, it is clear that this formulation will lead to values of the curvature in Equation 10 that are much closer to a constant than, e.g., the simple average $\kappa_{i+1/2} = (\kappa_i + \kappa_{i+1})/2$ often used for the classical level-set formulation. This has recently been confirmed by Abadie et al. (2015), who showed that the GFM/SSF level-set formulation leads to exact balance, in contrast to the classical level-set formulation, which gives significant spurious currents.

The benefits of ensuring a close-to-constant curvature estimate in the case of a spherical interface are also obvious for the alternative surface tension formulation in Equation 8, which has a built-in well-balanced property (irrespective, in this case, of the specific choice of gradient operators).

The main drawback of level-set formulations is the lack of discrete volume/mass conservation. This can be minimized by employing frequent redistancing and reinitialization of the level-set function. Unfortunately, this redistancing step tends to perturb the curvature and prevents the system from reaching the constant curvature required to guarantee exact balance (see Abadie et al. 2015).

## 4.2. Smoothed Volume Fraction

The normal and curvature relations (Equation 9) can, in principle, be applied to any field that provides an approximation of the interface position as a local isocontour. This was the observation that led Brackbill et al. (1992) to propose the original CSF model, in which the curvature is approximated using

$$\mathbf{n} = \frac{\nabla\tilde{c}}{|\nabla\tilde{c}|} \quad \text{and} \quad \kappa = \nabla\cdot\mathbf{n},$$

where $\tilde{c}$ is a smoothed (i.e., diffused) version of the sharp volume fraction field. The smoothing was adopted to try to circumvent the difficulty of differentiating a discontinuous function. Although results do improve when stronger diffusion is applied, several studies have since showed that this method is not consistent for curvature, i.e., errors on curvature tend to increase with spatial resolution (see, e.g., Williams et al. 1998, Cummins et al. 2005, Tryggvason et al. 2011). This inconsistency of the curvature estimate, often combined with the lack of balance of the gradient terms described above, explains most of the difficulties encountered with early CSF implementations. For many years, this has been a strong argument in favor of level-set methods, which, even for their naive, not-well-balanced versions, are at least consistent and give much better results for surface tension. Although this argument has often been repeated in recent publications, the smoothed volume fraction method should be considered obsolete because much better alternatives now exist, as described in the next section.



## 4.3. Height Functions

The height-function method relies on the simple observation that one can always define a local coordinate system in which a surface is described as the graph of a function. The simplest case is that of a nearly horizontal interface that can be simply described by $y = h_y(x)$ and for which the curvature is given by

$$\kappa = \frac{h_y''}{\sqrt{1 + h_y'^2}}.$$

Provided that the values of $h_y$ (the height function) are known exactly at discrete locations, one can easily derive discrete schemes to estimate $\kappa$ at any order of accuracy. This reasoning is easily generalized to any number of spatial dimensions. Of course, an issue arises when the slope of the interface tends to infinity and the graph becomes multivalued. One can then simply switch to a different, well-behaved local representation of the interface, such as $x = h_x(y)$.

This simple idea has a long history, possibly starting with Poo & Ashgriz (1989). It was first described comprehensively in the context of two-phase flows by Sussman (2003) and later analyzed in detail by Cummins et al. (2005). The key to the success of this method is having access to sufficiently accurate discrete values of the height function. Indeed, as double differentiation is required to estimate curvature, the height function needs to be known with higher than second-order accuracy to get a consistent (i.e., converging) estimate of the curvature. In the case of VOF methods, if we assume that the discrete volume fractions $c_{i,j}$ are known exactly [for example, using volume fractions obtained by analytical integration based on the exact interface (Bnà et al. 2015)], we can write without approximation

$$\int_{x_{i-1/2}}^{x_{i+1/2}} h_i(x)\,\mathrm{d}x = \Delta\overline{h_i} = \sum_{j=-\infty}^{j=\infty} c_{i,j} + \text{constant}, \qquad 12.$$

where $\overline{h_i}$ is the exact average height function value for a given column. The $\pm\infty$ limits of the sum on the right-hand side simply indicate that vertical summation of the volume fractions is performed on the entire column. A symmetric relation is, of course, derived for integration along rows, which allows one to perform the coordinate system rotation described above. Once these exact average values are computed, one can use simple differencing such as

$$\kappa_i = \frac{(\bar{h}_{i-1} - 2\bar{h}_i + \bar{h}_{i+1})/\Delta^2}{\sqrt{1 + [(\bar{h}_{i+1} - \bar{h}_{i-1})/(2\Delta)]^2}}$$

to obtain second-order accurate estimates of the curvature. Both second- and fourth-order convergence (using five-point stencils) have been demonstrated in practice for circular interfaces (Cummins et al. 2005, Sussman & Ohta 2006, Bornia et al. 2011). Generalization of the method to three dimensions is straightforward.

Besides its conceptual simplicity and good convergence properties, the method has several advantages that are particularly relevant in the context of the well-balanced property discussed above. First, the method naturally defines curvatures on the interface. Second, the method is insensitive to the exact distribution of volume fractions within a column. This is important for robustness because VOF schemes often lead to the formation of small interfacial fragments. Using these small fragments as markers of interface position can lead to erroneous curvature estimates (for example, when using the interpolation techniques described in Section 4.4). The spatial averaging performed by the height-function method naturally avoids these artifacts. Third, more generally, the connection between interface representation (and transport) and surface tension is very direct when combining VOF, balanced surface force discretization, such as Equation 6, and height-function curvature estimation: This tight coupling minimizes the possibility of uncontrolled numerical modes and gives a robust method.

Several issues must be addressed when implementing the method in practice, however. The summation limits on $j$ in Equation 12 need to be specified. Early implementations only used a fixed number of cells (typically seven) in each column. If one considers a nearly horizontal interface, described using a nondiffusive VOF method, only three cells in the vertical direction are necessary to obtain a consistent value for the average height. However, some interface configurations may require up to nine cells in the vertical direction to obtain consistent height functions (see, e.g., Popinet 2009 for a discussion and examples). More generally, although consistent height-function approximations can always be obtained when the spatial resolution is high enough (i.e., when the product $\kappa\Delta$ is small enough), things become more complicated as soon as this product is larger than approximately 1/5.

A first useful step is to use a variable stencil height, which adjusts automatically to the local topology of the interface, in order, in particular, to ensure that vertical summation is only applied across a single interface. This also permits the use of optimal stencils (e.g., three instead of seven cells) in the simpler cases (for examples of this approach, see López et al. 2009, Popinet 2009).

As spatial resolution decreases further, consistent height functions are increasingly difficult to obtain: When one reaches $\kappa\Delta \simeq 1$, at best a single value of the height function can be constructed in each direction, and differentiation to obtain curvature is no longer possible. Although one cannot reasonably expect accurate solutions at such low resolutions, it is important to ensure that the overall method remains robust across these transitions. This can be achieved by switching progressively to the interpolation methods described in the next section. A complete example of this approach was described by Popinet (2009). An alternative approach was proposed by Owkes & Desjardins (2015), who used a rotated height-function stencil.

## 4.4. Differential Geometry of Discrete Surfaces

The second class of methods for curvature estimation relies on an explicit, often local discretization of the surface. It is the natural method to use for front tracking, where the interface is defined explicitly, for example, using Lagrangian vertices connected by triangular facets.

The approximation of surfaces using discrete elements has many applications besides interfacial flows, such as three-dimensional laser scanning, mesh compression and denoising, minimal surfaces, and geodesics. Approximations of differential quantities, such as Gaussian and mean

curvatures or principal directions, have recently seen a surge of interest in the general context of computational geometry. An interesting review of the connections between the continuous mathematical concepts and their discrete equivalents is given by Meyer et al. (2003). They found the derivation of a discrete equivalent of the mean curvature normal operator, which is directly related to surface area minimization. This discrete operator mimics several of the important properties of the continuous operator; in particular, it minimizes a discrete version of the surface energy. Note that the techniques described in this review have not yet, as far as I am aware, been applied to front-tracking codes.

Besides this discrete formulation, two main types of techniques can be applied depending on whether a globally continuous approximation is required or a local approximation is sufficient. In global methods, local surface patches are constructed and continuity conditions are imposed between patches, which leads to the inversion of a system for the entire surface. Splines and B-splines belong to this family. In the context of interfacial flows, spline curves have been used, for example, by Popinet & Zaleski (1999), to connect Lagrangian markers in two dimensions, whereas B-splines have been used by Torres & Brackbill (2000) to obtain a global interface representation, also in two dimensions. These methods are accurate and benefit from the robustness provided by a global reconstruction [which can be seen as minimizing a global surface energy functional, i.e., the bending energy for 2D splines (Birkhoff & De Boor 1965)]; however, they are also expensive and complex, particularly in three dimensions.

In practice, local surface approximations are much more common. A standard technique is to approximate the surface by least-square minimization of the quadratic form

$$\sum_i w_i(\mathbf{x}_i \cdot \mathbf{A}\mathbf{x}_i + \mathbf{n} \cdot \mathbf{x}_i + b)^2, \qquad 13.$$

where $\mathbf{n}$ is a unit vector approximating the normal and $\mathbf{A}$ is a symmetric matrix. Further constraints can be used to reduce the number of free parameters. For example, Renardy & Renardy (2002) argued that one can get a consistent, second-order approximation by imposing the condition that the axis of the paraboloid defined by Equation 13 be aligned with $\mathbf{n}$, i.e., $\mathbf{An} = \mathbf{0}$. Popinet (2009) used a similar argument to reformulate the approximation problem in a local coordinate system aligned with $\mathbf{n}$. A sufficient number of points $\mathbf{x}_i$ are then chosen in a local neighborhood to make the system in Equation 13 invertible. The coefficients $w_i$ are optional ad hoc weights accounting for differences in accuracy of the positions. Besides the normal $\mathbf{n}$, the mean curvature is then given by $\kappa = 2\,\mathrm{tr}(\mathbf{A})$.

With the possible exception of triangulated surfaces of known connectivity (Tryggvason et al. 2001), it is clear that such local approximations are not nearly as simple or systematic as level sets or even height functions. Although the least-square minimization is not particularly complex or computationally expensive, the logic of point (and weight) selection can be complicated and somewhat fragile. Besides its application to front tracking, variants of this method have been used, in particular, in the parabolic reconstruction of surface tension (PROST) method of Renardy & Renardy (2002). In their article, it is not the discrete interface locations that are fitted through Equation 13, but the volume fractions given by the intersection of the quadratic surface with each cell of a local stencil. The resulting minimization problem is nonlinear and very expensive to solve numerically but provides accurate normal and curvature estimates directly from the volume fraction field. Ad hoc weighting is used to avoid computational modes and to increase the robustness of the method. Variants of this method have also been used in the generalized height-function method of Popinet (2009). As described above, when $\kappa\Delta < 1/5$, the number of consistent discrete heights may not be enough to allow differentiation. It is then necessary to use other types

of surface approximations. Ideally, switching from one approximation (e.g., height function) to the next (e.g., least-square minimization) should be done while minimizing the potential jumps in the estimated curvature. A first step is to obtain interface positions by combining horizontal and vertical heights and applying Equation 13. If the number of interface positions obtained in this way is too small, one can switch, as a last resort, to interface positions given directly by the VOF geometric reconstruction.

Popinet's (2009) application, and many subsequent ones, of the method to complex problems has shown that this method is both accurate and robust. The computational cost is limited because the relatively expensive least-square problems need to be solved only in marginal cases. The main cost is, rather, the added code complexity, which is, however, quite manageable (see, for example, Popinet 2014 for a complete open-source implementation).



## 4.5. Mixed Methods

The relative advantages and drawbacks of various methods have led to techniques seeking to combine several interface representations. The primary motivation was the improvement of interface kinematics, particularly their accuracy and mass conservation properties, but the accuracy of surface tension representation was also an important factor.

One of the better-known mixed methods is the coupled level-set and volume-of-fluid (CLSVOF) method of Sussman & Puckett (2000), which couples a geometric VOF representation (for conservative transport) with a level set (for simple curvature estimation). Many variants of this approach have since been developed and successfully applied to complex interfacial flow problems. The main weakness of this technique is common to all mixed methods: It is difficult to switch between interface representations without loss of accuracy on the interface position. These errors can become dominant when computing curvature. For example, Cummins et al. (2005) have analyzed the curvature errors induced by their reconstructed distance function (RDF) procedure, which is close to that employed in CLSVOF methods. Using a second-order-accurate RDF reconstruction, they demonstrated that, as expected, normals estimated from the RDF converge at a first-order rate, whereas curvature errors do not converge with resolution. More generally, one can expect that this reconstruction error will affect most types of redistancing algorithms used to ensure the consistency of level-set representations. This should be particularly clear when considering the well-balanced cases discussed above: In these cases, redistancing (or CLSVOF coupling) will lead to a continuous injection of curvature errors, which will prevent an equilibrium curvature from being reached. This assumption has been confirmed for the spurious currents test cases discussed in Section 6.1.

Another common class of mixed interface representations combines front tracking/Lagrangian particles with level set/isosurfaces/VOF. From a kinematic point of view, the goal is to combine the high accuracy of Lagrangian advection schemes with the topological flexibility of level-set/VOF interface representations. The improved kinematic properties of these schemes have been demonstrated by Enright et al. (2002) and Hieber & Koumoutsakos (2005) for particles combined with level set and Aulisa et al. (2003) for particles combined with VOF. The level contour reconstruction method (LCRM) of Shin et al. (2005) uses (temporary) interface markers reconstructed from the isosurface of the indicator (i.e., level-set) function. This eliminates the need to keep track of surface connectivity (i.e., topology) of standard front-tracking techniques. The curvature is computed using the local triangulated isosurface reconstruction, and surface tension is then implemented using balanced CSF applied to the indicator function. Although the convergence of curvature errors is not discussed by Shin et al. (2005) (one can expect the same difficulties as in the RDF method), good results are obtained for the spurious currents test cases.

## 5. STABILITY AND IMPLICIT TIME STEPPING

As first discussed briefly by Brackbill et al. (1992), a time-explicit discretization of the surface tension term should lead to a stability constraint of the form

$$\Delta t < \sqrt{\frac{(\rho_1 + \rho_2)\Delta^3}{4\pi\sigma}} \equiv \Delta t_\sigma, \qquad 14.$$

where $\Delta t$ is the time step and $\rho_1$ and $\rho_2$ are the densities on either side of the interface. The physical justification is that the time step must be small enough to resolve the fastest capillary waves in the system, which are obtained for the wave number $k = \pi/\Delta$, and verify the dispersion relation $c_\sigma = \sqrt{\sigma k/(\rho_1 + \rho_2)}$. A more formal stability analysis can be found, for example, in the work of Sussman & Ohta (2009). Note that the assumptions that lead to the $4\pi$ constant in Equation 14 are debatable (for a detailed discussion, see Galusinski & Vigneaux 2008, Denner & van Wachem 2015).

Explicit schemes for the transport of interfaces are subject to the standard CFL constraint $\Delta t < \Delta/|\mathbf{u}| \equiv \Delta t_{\text{adv}}$. The ratio of these two stability constraints is, thus,

$$\frac{\Delta t_\sigma}{\Delta t_{\text{adv}}} = \sqrt{\frac{(\rho_1 + \rho_2)|\mathbf{u}|^2\Delta}{4\pi\sigma}} = \sqrt{\text{We}_\Delta},$$

where $\text{We}_\Delta$ is the cell Weber number, which estimates the ratio of inertial to surface tension forces. In the absence of viscosity, the minimum characteristic scale (i.e., radius of curvature) of interfaces is due to the balance of inertial and surface tension forces. This implies that a well-resolved numerical simulation will necessarily verify $\text{We}_\Delta \ll 1$, so that the minimum characteristic scale of interfaces (e.g., minimum droplet size) is (much) larger than the mesh size. This means that the capillary time-step restriction $\Delta t_\sigma$ must always be more restrictive than the CFL constraint for interface advection. For example, if we consider a 1-mm air bubble rising in water with a terminal velocity of 0.1 m/s, we get

$$\frac{\Delta t_\sigma}{\Delta t_{\text{adv}}} = \sqrt{\text{We}_\Delta} = \sqrt{\text{We}_D} N^{-1/2} \approx 0.1 N^{-1/2},$$

where $\text{We}_D$ is the bubble Weber number (based on diameter $D$) and $N$ is the number of grid points per bubble diameter. For a moderate resolution of $N = 10$, the capillary time step is thus 32 times smaller than the advection time step.

One might wonder whether viscosity can relax the stability condition. This could be particularly relevant for small-scale flows, such as those occurring in microfluidics devices, and has been studied in this context by Galusinski & Vigneaux (2008). They concluded and demonstrated numerically that, for capillary-driven Stokes flows, the relevant stability criterion is

$$\Delta t < \max\left(\frac{\mu\Delta}{\sigma}, \sqrt{\frac{\rho\Delta^3}{\sigma}}\right),$$

where the first term corresponds to a CFL condition built with the Stokes velocity $\sigma/\mu$. The combined criterion thus becomes advantageous whenever the Stokes velocity is smaller than the speed of the shortest capillary waves, i.e., $\sigma/\mu < \sqrt{\sigma/\rho\Delta}$, which gives

$$\Delta < l_\mu = \frac{\mu^2}{\rho\sigma},$$

where $l_\mu$ is the viscocapillary length, which only depends on the fluid properties. As a reminder, we have $l_\mu \approx 14 \times 10^{-9}$ m and $\sigma/\mu \approx 72$ m/s for an air–water interface and $l_\mu \approx 2.5$ cm and $\sigma/\mu \approx 4.5$ cm/s for an air–glycerol interface. Note that microfluidics devices typically use mineral

oils, which have viscosities and surface tensions comparable to those of water and channel widths of the order of 10 μm. A well-resolved simulation will have a spatial resolution of order $\Delta \approx 0.1$ μm, which is still much larger than the viscocapillary length. It is thus not obvious that the relaxed Stokes criterion is beneficial for these applications, unless one considers significantly more viscous fluids or smaller channels. In practice, explicit surface tension stability is thus a stringent constraint for microfluidics applications (see Ling et al. 2016 for a detailed discussion).

Time-implicit discretizations are a standard way to relax time-step restrictions. Fast modes are damped rather than resolved and do not constrain the overall stability. One of the first articles discussing time-implicit schemes for surface tension was by Bänsch (2001), who proposed a variational formulation coupled with a Lagrangian finite-element discretization of the interface [see also the interesting review by Buscaglia & Ausas (2011)]. This was inspired by earlier work on the computation of minimal surfaces through discretization of the mean curvature flow equation (Dziuk 1990). Hysing (2006) extended these ideas to an Eulerian interface description. The scheme is derived starting from the standard differential geometry relation (Weatherburn 1927)

$$\underline{\boldsymbol{\Delta}}\mathbf{x}_s = \kappa\mathbf{n},$$

where $\mathbf{x}_s = \mathbf{x}\delta_s$ is the Lagrangian interface position and $\underline{\boldsymbol{\Delta}}$ is the Laplace-Beltrami operator (or surface Laplacian). The surface tension force can then be written

$$\mathbf{f}_\sigma = \sigma\kappa\mathbf{n}\delta_s = \sigma\underline{\boldsymbol{\Delta}}\mathbf{x}_s\delta_s.$$

The idea is to then use the interface position predicted at the next time step by

$$\mathbf{x}_{s,n+1} = \mathbf{x}_{s,n} + \Delta t\mathbf{u}_{n+1}$$

to obtain a semi-implicit discretization of the surface tension force as

$$\mathbf{f}_{n+1} = \sigma\,(\underline{\boldsymbol{\Delta}}\mathbf{x}_s)_{n+1}\,\delta_{s,n} = \sigma\,(\underline{\boldsymbol{\Delta}}\mathbf{x}_s)_n\,\delta_{s,n} + \Delta t\sigma\,(\underline{\boldsymbol{\Delta}}\mathbf{u})_{n+1}\,\delta_{s,n} = \sigma(\kappa\mathbf{n}\delta_s)_n + \Delta t\sigma\,(\underline{\boldsymbol{\Delta}}\mathbf{u})_{n+1}\,\delta_{s,n}.$$

The scheme is not fully implicit, particularly because the time level is not taken into account for $\delta_s$ (which is always defined at time $n$). The scheme is equivalent to the addition of a surface viscosity proportional to $\Delta t\sigma$ that will dampen fast capillary waves and lead to stabilization. Hysing (2006) demonstrated gains of one order of magnitude in time step compared to standard explicit schemes. The method is also applied in a finite-volume/VOF context by Raessi et al. (2009), who found similar stability properties.

More recently, Sussman & Ohta (2009) proposed to estimate the curvature at $n+1$ using the mean curvature flow equation

$$\partial_t\mathbf{x}_s = \sigma\kappa\mathbf{n} = \sigma\underline{\boldsymbol{\Delta}}\mathbf{x}_s \qquad 15.$$

rather than the full coupled Navier–Stokes system. The stationary solutions of this equation minimize the surface energy, which is clearly a desirable property when considering the stability of integrations with large time steps, for which they obtain the stability condition

$$\Delta t \leqslant \frac{\Delta(\rho_1+\rho_2)}{2\pi}. \qquad 16.$$

They then numerically demonstrate improved stability compared to the standard discretization, with increases in time step of the same order as for the method of Hysing (2006).

These two equations are problematic, however, because neither is dimensionally consistent. The analysis can be fixed by noting that Equation 15 is not an equation describing the evolution of an interface under the effect of surface tension, despite its connection with minimal surfaces. Indeed, dimensional consistency implies that the coefficient $\sigma$ in Equation 15 has dimensions $L^2T^{-1}$, i.e., those of a diffusion coefficient. The mean curvature flow equation (Equation 15) is

simply a surface diffusion equation that will filter high-frequency surface modes and, therefore, stabilize the solution. This is well known in the computer graphics community, where Equation 15 is used to denoise surface meshes (Desbrun et al. 1999).

The scheme can be reformulated consistently as the level-set evolution equation (Chopp 1993)

$$\partial_\tau \phi = \kappa, \qquad 17.$$

where the pseudo-time $\tau$ has the dimension of length squared. A filtered curvature can then be defined as

$$\tilde{\kappa} = \frac{1}{\Lambda^2}\int_0^{\Lambda^2} \kappa \, \mathrm{d}\tau = \frac{\phi(\Lambda^2) - \phi(0)}{\Lambda^2},$$

where $\phi(\Lambda^2)$ is obtained by advancing Equation 17 from zero to $\Lambda^2$, with $\Lambda$ a characteristic smoothing length. The amount of smoothing required is found by considering the linear stability of the resulting scheme, which gives the stability condition

$$\Lambda > \Delta t \sqrt{\frac{\sigma}{\Delta(\rho_1 + \rho_2)}} = \Delta t c_\Delta,$$

where $c_\Delta$ is the capillary wave speed for the (smallest) wavelength $\Delta$. The correct interpretation of the scheme of Sussman & Ohta (2009) is thus stabilization by diffusive surface smoothing over the characteristic travel distance of the fastest capillary waves: $\Lambda = \Delta t c_\Delta$.

The schemes of Sussman & Ohta (2009) and Hysing (2006) thus work in a similar manner: Added surface damping filters high-frequency modes and thus stabilizes the solution. An important difference between the two schemes, however, is that the method of Sussman & Ohta directly filters the interface position/curvature while the scheme of Hysing filters the (surface) velocity field. In particular, the scheme of Hysing will not affect equilibrium shapes for which $\mathbf{u} = 0$, but the scheme of Sussman & Ohta will. More generally, these schemes are not very scale-selective filters (because they are both based on low-order differential operators), i.e., they will also significantly dampen lower-frequency modes that do not restrict stability.

Pushing this approach further, one can devise, at least formally, near-optimal filtering schemes. If we consider the simpler case of a one-dimensional interface defined through its graph $\eta(x,t)$, the Fourier transform of the corresponding curvature is given by

$$\hat{\kappa}(k,t) = -k^2 \hat{\eta}(k,t),$$

where $\hat{\eta}(k,t)$ is the Fourier transform of the interface position and where we have assumed a vanishing interface slope. An optimal filtered curvature can then be defined in Fourier space as

$$\tilde{\kappa}(k,t) = \min\left(1, \frac{\rho_1 + \rho_2}{\sigma k^3 \Delta t^2}\right)\hat{\kappa}(k,t).$$

Computing the inverse Fourier transform and using the resulting filtered curvature will then ensure stability of the explicit scheme. The filtering is optimal because only the necessary (mode-dependent) amount of damping is added. This scheme works well in practice, for example, using fast Fourier transforms (FFTs) for periodic graphs in one or two dimensions; however, generalizing it to more complex topologies seems difficult. For front-tracking interface representations, spectral mesh processing could be a solution (see Lévy & Zhang 2010 for an interesting introduction).

## 6. TEST CASES

Test cases are important for the development and assessment of new numerical schemes. Cross-referencing publicly accessible automated test suites (for examples, see Popinet 2003, Popinet et al.

2013) with journal articles is also an excellent way of ensuring reproducibility and independent peer review of the numerical results. In this section, I try to point out a minimal set of test cases for surface tension models, as well as their shortcomings and common pitfalls.

## 6.1. Laplace's Equilibrium and Spurious Currents

Laplace balance between surface tension and pressure gradient provides a trivial equilibrium solution that is, nevertheless, difficult to reproduce numerically, leading to the production of numerical artifacts, the so-called spurious or parasitic currents. This was first observed and discussed in detail in the context of lattice Boltzmann methods for two-phase flows (Gustensen 1992), and many variants of this test case have since appeared in the literature.

An important issue is that of the timescale required to reach equilibrium. There are two natural timescales in this simple system: the period of oscillation scaling, i.e., $T_\sigma = \sqrt{\rho D^3/\sigma}$, where $D$ is the droplet diameter, and the viscous dissipation timescale $T_\mu = \rho D^2/\mu$. The ratio of these two timescales is $T_\sigma/T_\mu = \mu/\sqrt{\rho\sigma D}$, the Ohnesorge number. To reach the asymptotic regime corresponding to the equilibrium solution, one then needs to make sure that the simulations are run on a timescale (much) larger than either of these two timescales. Detailed parameters for such a setup are provided, for example, by Lafaurie et al. (1994) and Popinet & Zaleski (1999).

Note that many studies have been published that do not verify this condition of asymptotic convergence. For example, Francois et al. (2006) used a version of this test where a few time steps, or even a single time step, are performed before measuring the amplitude of spurious currents. In the case of well-balanced schemes, the cause of spurious currents after a few time steps is only the deviation from constant of the initial curvature computed by the scheme. This deviation is better characterized by, for example, a convergence test on the curvature estimate for a spherical interface (see, e.g., Cummins et al. 2005, Popinet 2009), without running the risk of confusing several properties of the scheme (i.e., balance versus curvature estimation).

However, if the test respects the asymptotic conditions $t > T_\mu$ and $t > T_\sigma$, one expects a consistent, well-balanced method to converge toward an interfacial shape that will ensure exact equilibrium (i.e., $\mathbf{u} = 0$ to within machine accuracy). This interfacial shape may not itself be exact (i.e., an exact circle or sphere), and the evolution of the velocity around the interface is expected to reflect the physical evolution (through damped capillary waves) from the initial perturbed condition toward the numerical equilibrium solution. Of course, one expects this numerical equilibrium interface shape to converge toward the exact equilibrium (circular) shape as spatial resolution is increased. Popinet (2009) demonstrated this convergence in the case of the VOF and height-function–CSF surface tension method. Note that such a convergence is not trivial, however, because it requires that the scheme guarantee evolution toward a constant curvature.

In an important extension of this test proposed by Popinet (2009), a constant background velocity field ensures uniform translation of the droplet across the grid in a spatially periodic domain. Laplace's equilibrium solution is, of course, still valid in the frame of reference of the droplet. This test is more relevant to practical applications, particularly when considering low-velocity and high-surface-tension cases such as microfluidics or multiphase flow through porous media. This test was used extensively in the interesting comparative study of Abadie et al. (2015), who underlined the detrimental effect of interface (and curvature) perturbations induced by either interfacial transport (for VOF) or redistancing and interface reconstruction (for level set and coupled level set/VOF) (see also the demonstration of consistent balance for level-set methods without redistancing in Abadie et al. 2015, section 5).

## 6.2. Capillary Oscillations

Capillary oscillations around equilibrium solutions are the next logical step. Analytical solutions can be obtained through classical linear stability analysis in the limit of vanishing amplitude and viscosity for both planar and circular or spherical interfaces (Lamb 1932). Fyfe et al. (1988) considered the oscillation of a two-dimensional elliptical droplet in an inviscid fluid, for which the oscillation frequency is given by

$$\omega_n = (n^3 - n)\frac{\sigma}{(\rho_1 + \rho_2)a^3}, \qquad 18.$$

where the droplet shape is given in polar coordinates by $r = a + \epsilon \cos(n\theta)$. This is an extension to two phases of a result by Rayleigh (1879), who considered the stability of the cross section of a jet. Although many variants of this test case exist, one of the most challenging is for large density ratios (1/1,000) without viscosity. Details can be found in, e.g., the work of Torres & Brackbill (2000), Herrmann (2008), and Fuster et al. (2009). The total energy (surface plus kinetic) should remain constant, and any decay is a sign of numerical dissipation, which should be minimized. Conversely, increasing total energy is a clear signature of surface tension imbalance. This setup is a stringent test of the accuracy of the surface tension representation because physical or numerical viscosity cannot intervene to limit spurious currents. In addition to minimizing dissipation, good numerical schemes can give second-order spatial convergence in the estimated oscillation frequency compared to Equation 18 (see Fuster et al. 2009 for results with different schemes).

Analytical solutions can also be obtained when viscosity is taken into account. The simplest analysis leads to exponential damping of oscillating modes; however, as studied in detail by Prosperetti (1981), this gives significant deviations (several percent) compared to initial-value solutions, taking into account the time dependence of vorticity diffusion into the medium. Prosperetti (1980, 1981) derived closed-form solutions for the Laplace transform of shape evolution for both planar and spherical interfaces. These solutions are the basis for a now-classical test case, first proposed by Popinet & Zaleski (1999), which considers the oscillations of a linearly perturbed, planar interface. Although less stringent than the inviscid case, due to a simpler geometry that is less affected by imbalance and spurious currents, this test evaluates the quality of the full coupling between interfacial motion, surface tension, viscosity, and inertia. Again, good schemes can demonstrate second-order convergence toward the analytical solution with a small prefactor (see Popinet 2009 for a comparison of different schemes).

## 6.3. More Complex Test Cases

Simple-looking test cases, for which analytical solutions exist, are often the most challenging, as illustrated by the history of spurious currents. More complex test cases are also useful, however, particularly for assessing practical applicability, including speed and robustness, of numerical schemes. An important issue for these tests is the availability of reference solutions. Analytical solutions are usually not available or have restrictions (e.g., on amplitudes or Reynolds numbers) that can be difficult to enforce in numerical simulations; experimental reference data may be available, but error bars may be large, and the experiments often include physical effects (e.g., surfactants, temperature gradients, or compressibility) that complicate their comparison with simpler numerical models. A popular example of this class is the case of rising bubbles, often used for validation of surface tension models. Due to a lack of accurate reference solutions, the validation is often qualitative, with a visual comparison of the shapes obtained experimentally or numerically. Although this was useful when methods were inaccurate enough to cause obvious departure from the expected solutions (for example, the extreme case of bubbles bursting due

to spurious currents), this is insufficient to assess the relative accuracies of modern numerical methods. A useful approach, which requires substantial effort, is to provide accurate, converged, numerical reference solutions for nontrivial problems. For example, Hysing et al. (2009) and Turek et al. (2008) gave reference solutions, using different numerical methods, for rising bubbles that can be reproduced accurately by other methods (see `rising.c` in Popinet et al. 2013). A similar effort was made for Taylor bubble solutions by Marschall et al. (2014) and Abadie et al. (2015).

## 7. SELECTED APPLICATIONS

Numerical simulations are particularly useful in combination with laboratory experiments. Their advantages and drawbacks are often complementary, so that simultaneous design of laboratory and numerical experiments can lead to deeper insight into complex physical phenomena. **Figure 2** illustrates an example of this approach. A millimeter-sized water droplet impacts on a pool and creates a complex splash structure. **Figure 2*a*** illustrates a close-up view of the impact zone, seen as a vertical cut through the center of the drop. This configuration was studied in detail both numerically and experimentally by Thoraval et al. (2012). The experiment and the numerical simulation are both very challenging due to the wide range of spatial scales and the short duration of the phenomenon. Care was taken to ensure converged axisymmetric simulations. This

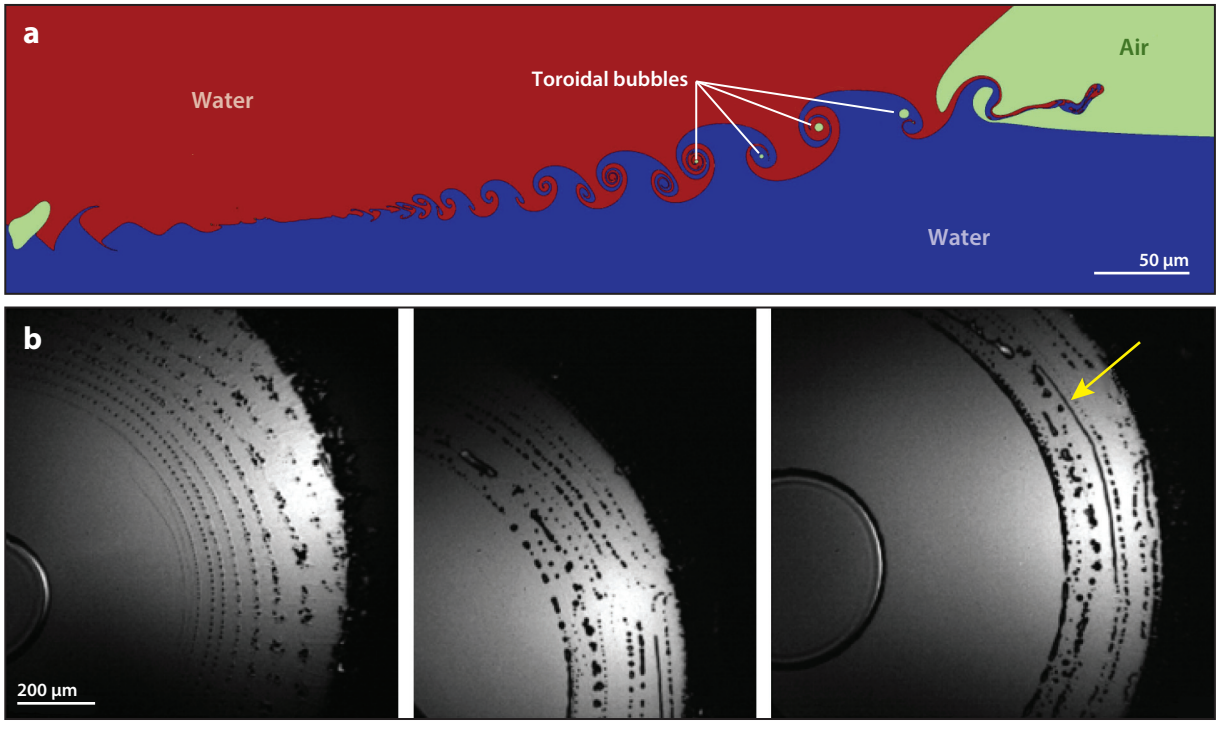


**Figure 2**

(*a*) Side view of an axisymmetric numerical simulation of the von Kármán vortex street created by the impact of a millimetric water droplet impacting on a pool. The axis of revolution is aligned with the left border of the image. The pool is colored in blue and the droplet in red for visualization purposes, but there are only two fluids: water and air (*light green*). (*b*) High-speed experimental imaging of the bubble rings (*yellow arrow*) created by the vortex street for different pool depths. Figure adapted with permission from Thoraval et al. (2013, figures 10 and 11).

required spatial resolutions of order $10^4$ grid points per drop diameter, i.e., resolved structures of order 1 μm. Besides an accurate surface tension model (well-balanced, height-function VOF-CSF), several numerical ingredients were necessary: adaptive mesh refinement, efficient multigrid pressure solver, and parallelism (Popinet 2009, Agbaglah et al. 2011). The numerical results were very consistent with experimental observations for the whole range of impact regimes (see also Agbaglah et al. 2015 for an impressive comparison with high-speed X-ray imaging), but predicted a regime characterized by the unexpected von Kármán vortex street of **Figure 2**. This is associated with complex dynamics of the ejecta sheet, which periodically entraps toroidal air bubbles. This regime was not observable using the side-view camera of the original experimental setup. This numerical result led to the redesign of the experiment to use bottom-view cameras with the goal of observing the bubble rings predicted by the numerics (Thoraval et al. 2013). A sample of the images obtained is illustrated in **Figure 2*b*** for different pool depths. Although the subsequent three-dimensional breakup of the toroidal bubbles (some of them are still intact in the right-most frame of **Figure 2*b***) cannot be predicted by the axisymmetric simulations, the experimental results spectacularly confirmed the numerical discovery.

The motion of gas bubbles in a liquid is a canonical example of the subtle balance among surface tension and viscous and buoyancy forces. The transitions between various regimes (straight, zigzag, or spiraling ascent) are particularly difficult to capture, either experimentally or numerically. They have been investigated numerically in a recent series of articles by Cano-Lozano et al. (2015, 2016). In contrast with the previous example, full three-dimensional simulations are necessary. The boundaries between regimes are controlled by the coupled interaction of the shape of the deformable bubble and the associated vorticity generation and wake formation. An example of the resulting trajectory, wake structure, and bubble shapes is given in **Figure 3**. Accurate modeling of surface tension is vital to minimize spurious vorticity generation at the interface. As in the previous study, Cano-Lozano et al. (2016) were careful to check the numerical convergence of their results. This required a resolution of 128 grid points per bubble diameter. A very large tank of $8 \times 8 \times 128$ diameters is necessary to be able to follow the bubble for a long time. This leads to formidable resolution requirements: $2^{34} \simeq 17$ billion grid points on a regular grid! Adaptive mesh refinement brings this down to around 10 million grid points and makes the simulations possible but still expensive (see **http://basilisk.fr/src/examples/bubble.c** for a full example). A large number of time steps is necessary to capture the transition to established regime, in particular because of the explicit time-step restriction discussed above. Note also that the parameters chosen correspond to those for a millimetric air bubble rising in a liquid roughly 10 times more viscous than water. Further refinement would be necessary to properly capture the boundary layers for an air–water bubble.

These two examples illustrate the capabilities, as well as limitations, of state-of-the-art models of surface tension. Obtaining numerically converged results clearly requires considerable computing power. This is feasible but challenging for complex two-dimensional (or axisymmetric) configurations. Provided care is taken, very valuable insight can be gained from such simulations (for a small representative sample, see, e.g., Samanta et al. 2011, Fuster et al. 2013, Hoepffner & Paré 2013, Deike et al. 2015).

In three dimensions, only relatively simple configurations can be studied with confidence that results are fully independent from the numerics. That said, the situation was similar for two-dimensional simulations 15 years ago, with the added limitation of less accurate surface tension models. Under-resolved three-dimensional simulations can still give very useful qualitative results for flows that are challenging to study experimentally, provided one controls for the effect of resolution and checks consistency with the available experimental data and theoretical models.

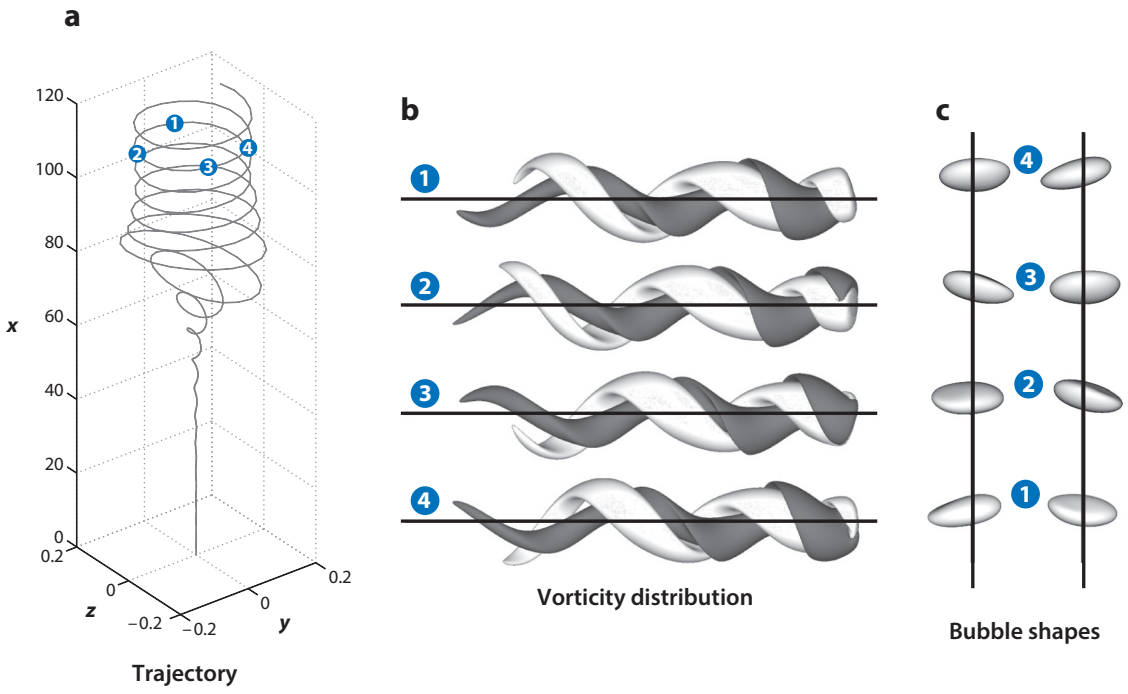


**Figure 3**

Numerical simulation of the (*a*) trajectory (units are bubble diameters), (*b*) vorticity distribution, and (*c*) shapes of a gas bubble rising in a liquid in the spiraling regime. The density ratio is close to air and water. The Galileo and Bond numbers are 100.25 and 10, respectively. Figure adapted with permission from Cano-Lozano et al. (2016, figures 10 and 11).

Representative examples of this approach include studies of atomization (Herrmann 2010, Chen et al. 2013, Desjardins et al. 2013, Jain et al. 2015, Ling et al. 2017), industrial processes (Mencinger et al. 2015), and waves (Deike et al. 2016). A balanced trio of experimental, theoretical, and numerical approaches can be extremely effective, and I expect numerical models of surface tension to play an important role in future advances in our understanding of complex multiphase flows.

## FUTURE ISSUES

1. None of the methods presented in this review satisfy both balance and momentum conservation, properties that are required for consistency and robustness. Integral formulations, which have been relatively neglected, could be a promising research direction.
2. Although high-order height-function schemes have been demonstrated for curvature estimation, current volumetric formulations are formally first-order accurate. This follows from detailed analysis of Peskin's scheme by LeVeque & Li (1994). Although immersed interface schemes have been extended to the second order (LeVeque & Li 1994, 1997; Peskin 2002; Xu & Wang 2006), they have so far only been applied to Lagrangian interface discretizations and fluid–structure interactions. Their generalization to generic two-phase flows, with an implicit interface representation, remains an open question.

3. Robust time-implicit schemes have already been formulated for Lagrangian immersed interface methods (Mayo & Peskin 1992, Newren et al. 2007), and there is no reason to believe that these results cannot be generalized to surface tension; however, recent efforts in this direction have yielded somewhat confusing results (Denner & van Wachem 2015).
4. Extensions to more than two phases, including the consistent treatment of triple points or lines, have only been considered recently (see, e.g., Li et al. 2015).
5. The schemes described in this review, and especially the height-function method, are most easily implemented on regular Cartesian grids (or their adaptive versions). Their generalization to unstructured grids, usually favored for industrial applications, has so far concentrated on kinematics rather than dynamics. Surface tension schemes on these grids, often based on diffuse algebraic VOF formulations, are currently quite limited compared to the state of the art on regular grids.
6. Finally, efforts should be pursued to provide standardized, benchmark cases showing numerical convergence (even if only first order) for relevant, nontrivial physical configurations.



## DISCLOSURE STATEMENT

The author is not aware of any biases that might be perceived as affecting the objectivity of this review.

## ACKNOWLEDGMENTS

I would like to thank all the colleagues and friends who made this review possible, especially Patrick Ballard, Christophe Josserand, Yue Ling, Yves Pomeau, Pascal Ray, Marie-Jean Thoraval, and Stéphane Zaleski.

## LITERATURE CITED

Abadie T, Aubin J, Legendre D. 2015. On the combined effects of surface tension force calculation and interface advection on spurious currents within volume of fluid and level set frameworks. *J. Comput. Phys.* 297:611–36

Agbaglah G, Delaux S, Fuster D, Hoepffner J, Josserand C, et al. 2011. Parallel simulation of multiphase flows using octree adaptivity and the volume-of-fluid method. *C. R. Méc.* 339:194–207

Agbaglah G, Thoraval MJ, Thoroddsen ST, Zhang LV, Fezzaa K, Deegan RD. 2015. Drop impact into a deep pool: vortex shedding and jet formation. *J. Fluid Mech.* 764:R1

Anderson DM, McFadden GB, Wheeler AA. 1998. Diffuse-interface methods in fluid mechanics. *Annu. Rev. Fluid Mech.* 30:139–65

Aristotle. 1922 (350 BC). *The Works of Aristotle Translated into English*, Vol. IV, 313a: *De Caelo*, transl. JL Stock. Oxford, UK: Clarendon

Audusse E, Bouchut F, Bristeau MO, Klein R, Perthame B. 2004. A fast and stable well-balanced scheme with hydrostatic reconstruction for shallow water flows. *SIAM J. Sci. Comput.* 25:2050–65

Aulisa E, Manservisi S, Scardovelli R. 2003. A mixed markers and volume-of-fluid method for the reconstruction and advection of interfaces in two-phase and free-boundary flows. *J. Comput. Phys.* 188:611–39

Bänsch E. 2001. Finite element discretization of the Navier–Stokes equations with a free capillary surface. *Numer. Math.* 88:203–35

Birkhoff G, De Boor CR. 1965. Piecewise polynomial interpolation and approximation. *Approx. Funct.* 1965:164–90

Bnà S, Manservisi S, Scardovelli R, Yecko P, Zaleski S. 2015. Numerical integration of implicit functions for the initialization of the VOF function. *Comput. Fluids* 113:42–52

Bornia G, Cervone A, Manservisi S, Scardovelli R, Zaleski S. 2011. On the properties and limitations of the height function method in two-dimensional Cartesian geometry. *J. Comput. Phys.* 230:851–62

Brackbill J, Kothe DB, Zemach C. 1992. A continuum method for modeling surface tension. *J. Comput. Phys.* 100:335–54

Buscaglia GC, Ausas RF. 2011. Variational formulations for surface tension, capillarity and wetting. *Comput. Methods Appl. Mech. Eng.* 200:3011–25

Cano-Lozano JC, Bolaños-Jiménez R, Gutiérrez-Montes C, Martínez-Bazán C. 2015. The use of volume of fluid technique to analyze multiphase flows: specific case of bubble rising in still liquids. *Appl. Math. Model.* 39:3290–305

Cano-Lozano JC, Martínez-Bazán C, Magnaudet J, Tchoufag J. 2016. Paths and wakes of deformable nearly spheroidal rising bubbles close to the transition to path instability. *Phys. Rev. Fluids* 1:053604

Chen X, Ma D, Yang V, Popinet S. 2013. High-fidelity simulations of impinging jet atomization. *At. Sprays* 23:1079–101

Chopp DL. 1993. Computing minimal surfaces via level set curvature flow. *J. Comput. Phys.* 106:77–91

Cummins SJ, Francois MM, Kothe DB. 2005. Estimating curvature from volume fractions. *Comput. Struct.* 83:425–34

Deike L, Melville WK, Popinet S. 2016. Air entrainment and bubble statistics in breaking waves. *J. Fluid Mech.* 801:91–129

Deike L, Popinet S, Melville WK. 2015. Capillary effects on wave breaking. *J. Fluid Mech.* 769:541–69

Denner F, van Wachem BG. 2015. Numerical time-step restrictions as a result of capillary waves. *J. Comput. Phys.* 285:24–40

Desbrun M, Meyer M, Schröder P, Barr AH. 1999. Implicit fairing of irregular meshes using diffusion and curvature flow. *Proc. Annu. Conf. Comput. Graph. Interact. Tech., 26th, Los Angeles*, pp. 317–24. New York: ACM Press

Desjardins O, McCaslin J, Owkes M, Brady P. 2013. Direct numerical and large-eddy simulation of primary atomization in complex geometries. *At. Sprays* 23:1001–48

Desjardins O, Moureau V, Pitsch H. 2008. An accurate conservative level set/ghost fluid method for simulating turbulent atomization. *J. Comput. Phys.* 227:8395–416

Dziuk G. 1990. An algorithm for evolutionary surfaces. *Numer. Math.* 58:603–11

Engquist B, Tornberg AK, Tsai R. 2005. Discretization of Dirac delta functions in level set methods. *J. Comput. Phys.* 207:28–51

Enright D, Fedkiw R, Ferziger J, Mitchell I. 2002. A hybrid particle level set method for improved interface capturing. *J. Comput. Phys.* 183:83–116

Fedkiw RP, Aslam T, Merriman B, Osher S. 1999. A non-oscillatory Eulerian approach to interfaces in multimaterial flows (the ghost fluid method). *J. Comput. Phys.* 152:457–92

Francois MM, Cummins SJ, Dendy ED, Kothe DB, Sicilian JM, Williams MW. 2006. A balanced-force algorithm for continuous and sharp interfacial surface tension models within a volume tracking framework. *J. Comput. Phys.* 213:141–73

Fuster D, Agbaglah G, Josserand C, Popinet S, Zaleski S. 2009. Numerical simulation of droplets, bubbles and waves: state of the art. *Fluid Dyn. Res.* 41:065001

Fuster D, Matas JP, Marty S, Popinet S, Hoepffner J, et al. 2013. Instability regimes in the primary breakup region of planar coflowing sheets. *J. Fluid Mech.* 736:150–76

Fyfe DE, Oran ES, Fritts M. 1988. Surface tension and viscosity with Lagrangian hydrodynamics on a triangular mesh. *J. Comput. Phys.* 76:349–84

Galusinski C, Vigneaux P. 2008. On stability condition for bifluid flows with surface tension: application to microfluidics. *J. Comput. Phys.* 227:6140–64

Gauss CF. 1830. *Principia Generalia Theoriae Figurae Fluidorum in Statu Aequilibrii*. Göttingen, Ger.: Dieterichs

Ghidaglia JM. 2016. Capillary forces: a volume formulation. *Eur. J. Mech. Fluids* 59:86–89

Gueyffier D, Li J, Nadim A, Scardovelli R, Zaleski S. 1999. Volume-of-fluid interface tracking with smoothed surface stress methods for three-dimensional flows. *J. Comput. Phys.* 152:423–56
Gustensen AK. 1992. *Lattice-Boltzmann studies of multiphase flow through porous media*. Ph.D. Thesis, Mass. Inst. Technol, Cambridge, MA
Harlow FH, Welch JE. 1965. Numerical calculation of time-dependent viscous incompressible flow of fluid with free surface. *Phys. Fluids* 8:2182–89
Herrmann M. 2008. A balanced force refined level set grid method for two-phase flows on unstructured flow solver grids. *J. Comput. Phys.* 227:2674–706
Herrmann M. 2010. Detailed numerical simulations of the primary atomization of a turbulent liquid jet in crossflow. *J. Eng. Gas Turbines Power* 132:061506
Hieber SE, Koumoutsakos P. 2005. A Lagrangian particle level set method. *J. Comput. Phys.* 210:342–67
Hoepffner J, Paré G. 2013. Recoil of a liquid filament: escape from pinch-off through creation of a vortex ring. *J. Fluid Mech.* 734:183–97
Hysing SR. 2006. A new implicit surface tension implementation for interfacial flows. *Int. J. Numer. Methods Fluids* 51:659–72
Hysing SR, Turek S, Kuzmin D, Parolini N, Burman E, et al. 2009. Quantitative benchmark computations of two-dimensional bubble dynamics. *Int. J. Numer. Methods Fluids* 60:1259–88
Jain M, Prakash RS, Tomar G, Ravikrishna R. 2015. Secondary breakup of a drop at moderate Weber numbers. *Proc. R. Soc. Math. Phys. Eng. Sci.* 471:20140930
Kang M, Fedkiw RP, Liu XD. 2000. A boundary condition capturing method for multiphase incompressible flow. *J. Sci. Comput.* 15:323–60
Lafaurie B, Nardone C, Scardovelli R, Zaleski S, Zanetti G. 1994. Modelling merging and fragmentation in multiphase flows with SURFER. *J. Comput. Phys.* 113:134–47
Lamb H. 1932. *Hydrodynamics*. Cambridge, UK: Cambridge Univ. Press
LeVeque RJ. 1998. Balancing source terms and flux gradients in high-resolution Godunov methods: the quasi-steady wave-propagation algorithm. *J. Comput. Phys.* 146:346–65
LeVeque RJ, Li Z. 1994. The immersed interface method for elliptic equations with discontinuous coefficients and singular sources. *SIAM J. Numer. Anal.* 31:1019–44
LeVeque RJ, Li Z. 1997. Immersed interface methods for Stokes flow with elastic boundaries or surface tension. *SIAM J. Sci. Comput.* 18:709–35
Lévy B, Zhang HR. 2010. Spectral mesh processing. In *ACM SIGGRAPH 2010 Courses*, ed. JL Mohler, art. 8. Los Angeles: ACM Press. **https://doi.org/10.1145/1837101.1837109**
Li G, Lian Y, Guo Y, Jemison M, Sussman M, et al. 2015. Incompressible multiphase flow and encapsulation simulations using the moment-of-fluid method. *Int. J. Numer. Methods Fluids* 79:456–90
Ling Y, Fullana JM, Popinet S, Josserand C. 2016. Droplet migration in a Hele–Shaw cell: effect of the lubrication film on the droplet dynamics. *Phys. Fluids* 28:062001
Ling Y, Fuster D, Zaleski S, Tryggvason G. 2017. Spray formation in a quasiplanar gas-liquid mixing layer at moderate density ratios: a numerical closeup. *Phys. Rev. Fluids* 2:014005
López J, Zanzi C, Gómez P, Zamora R, Faura F, Hernández J. 2009. An improved height function technique for computing interface curvature from volume fractions. *Comput. Methods Appl. Mech. Eng.* 198:2555–64
Mahady K, Afkhami S, Kondic L. 2016. A numerical approach for the direct computation of flows including fluid-solid interaction: modeling contact angle, film rupture, and dewetting. *Phys. Fluids* 28:062002
Marschall H, Boden S, Lehrenfeld C, Hampel U, Reusken A, et al. 2014. Validation of interface capturing and tracking techniques with different surface tension treatments against a Taylor bubble benchmark problem. *Comput. Fluids* 102:336–52
Maxwell JC. 1889. Capillary action. In *Scientific Papers of James Clerk Maxwell*, Vol. 2, ed. WD Niven, pp. 541–91. New York: Dover
Mayo AA, Peskin CS. 1992. An implicit numerical method for fluid dynamics problems with immersed elastic boundaries. *Contemp. Math.* 141:261–77
Mencinger J, Bizjan B, Širok B. 2015. Numerical simulation of ligament-growth on a spinning wheel. *Int. J. Multiph. Flow* 77:90–103
Mesinger F. 1982. On the convergence and error problems of the calculation of the pressure gradient force in sigma coordinate models. *Geophys. Astrophys. Fluid Dyn.* 19:105–17

Meyer M, Desbrun M, Schröder P, Barr AH. 2003. Discrete differential-geometry operators for triangulated 2-manifolds. In *Visualization and Mathematics*, Vol. III, ed. H-C Hege, K Polthier, pp. 35–57. Berlin: Springer

Newren EP, Fogelson AL, Guy RD, Kirby RM. 2007. Unconditionally stable discretizations of the immersed boundary equations. *J. Comput. Phys.* 222:702–19

Owkes M, Desjardins O. 2015. A mesh-decoupled height function method for computing interface curvature. *J. Comput. Phys.* 281:285–300

Peskin CS. 1972. Flow patterns around heart valves: a numerical method. *J. Comput. Phys.* 10:252–71

Peskin CS. 2002. The immersed boundary method. *Acta Numer.* 11:479–517

Pomeau Y. 2013. Surface tension: from fundamental principles to applications in liquids and in solids. *Proc. Warsaw School Stat. Phys., 5th, Kazimierz Dolny, Pol.*, pp. 1–33. Warsaw: Warsaw Univ. Press

Poo J, Ashgriz N. 1989. A computational method for determining curvatures. *J. Comput. Phys.* 84:483–91

Popinet S. 2003. *Test suite*. Gerris Softw. **http://gerris.dalembert.upmc.fr/gerris/tests/tests/index.html**

Popinet S. 2009. An accurate adaptive solver for surface-tension-driven interfacial flows. *J. Comput. Phys.* 228:5838–66

Popinet S. 2014. *Basilisk*. Basilisk Softw. **http://basilisk.fr/src/curvature.h**

Popinet S, Fullana J-M, Kirstetter G, Lagrée P-Y, Lopez-Herrera J, De Vita F. 2013. *Test cases*. Basilisk Softw. **http://basilisk.fr/src/test/README**

Popinet S, Zaleski S. 1999. A front-tracking algorithm for accurate representation of surface tension. *Int. J. Numer. Methods Fluids* 30:775–93

Prosperetti A. 1980. Free oscillations of drops and bubbles: the initial-value problem. *J. Fluid Mech.* 100:333–47

Prosperetti A. 1981. Motion of two superposed viscous fluids. *Phys. Fluids* 24:1217–23

Raessi M, Bussmann M, Mostaghimi J. 2009. A semi-implicit finite volume implementation of the CSF method for treating surface tension in interfacial flows. *Int. J. Numer. Methods Fluids* 59:1093–110

Rayleigh JW. 1879. On the capillary phenomena of jets. *Proc. R. Soc.* 29:71–97

Renardy Y, Renardy M. 2002. PROST: a parabolic reconstruction of surface tension for the volume-of-fluid method. *J. Comput. Phys.* 183:400–21

Samanta A, Ruyer-Quil C, Goyeau B. 2011. A falling film down a slippery inclined plane. *J. Fluid Mech.* 684:353–83

Scardovelli R, Zaleski S. 1999. Direct numerical simulation of free-surface and interfacial flow. *Annu. Rev. Fluid Mech.* 31:567–603

Sethian JA, Smereka P. 2003. Level set methods for fluid interfaces. *Annu. Rev. Fluid Mech.* 35:341–72

Shin S, Abdel-Khalik S, Daru V, Juric D. 2005. Accurate representation of surface tension using the level contour reconstruction method. *J. Comput. Phys.* 203:493–516

Sussman M. 2003. A second order coupled level set and volume-of-fluid method for computing growth and collapse of vapor bubbles. *J. Comput. Phys.* 187:110–36

Sussman M, Ohta M. 2006. High-order techniques for calculating surface tension forces. In *Free Boundary Problems: Theory and Applications*, ed. P Colli, C Verdi, A Visintin, pp. 425–34. Berlin: Springer

Sussman M, Ohta M. 2009. A stable and efficient method for treating surface tension in incompressible two-phase flow. *SIAM J. Sci. Comput.* 31:2447–71

Sussman M, Puckett EG. 2000. A coupled level set and volume-of-fluid method for computing 3D and axisymmetric incompressible two-phase flows. *J. Comput. Phys.* 162:301–37

Sussman M, Smereka P, Osher S. 1994. A level set approach for computing solutions to incompressible two-phase flow. *J. Comput. Phys.* 114:146–59

Thoraval MJ, Takehara K, Etoh TG, Popinet S, Ray P, et al. 2012. Von Kármán vortex street within an impacting drop. *Phys. Rev. Lett.* 108:264506

Thoraval MJ, Takehara K, Etoh TG, Thoroddsen ST. 2013. Drop impact entrapment of bubble rings. *J. Fluid Mech.* 724:234–58

Torres D, Brackbill J. 2000. The point-set method: front-tracking without connectivity. *J. Comput. Phys.* 165:620–44

Tryggvason G, Bunner B, Esmaeeli A, Juric D, Al-Rawahi N, et al. 2001. A front-tracking method for the computations of multiphase flow. *J. Comput. Phys.* 169:708–59

Tryggvason G, Scardovelli R, Zaleski S. 2011. *Direct Numerical Simulations of Gas–Liquid Multiphase Flows*. Cambridge, UK: Cambridge Univ. Press

Turek S, Becker C, Kilian S, Möller M, Buijssen S, et al. 2008. *Bubble benchmark*. Featflow Softw. **http://www.featflow.de/en/benchmarks/cfdbenchmarking/bubble.html**

Unverdi SO, Tryggvason G. 1992. A front-tracking method for viscous, incompressible, multi-fluid flows. *J. Comput. Phys.* 100:25–37

Weatherburn CE. 1927. *Differential Geometry of Three Dimensions*, Vol. 1. Cambridge, UK: Cambridge Univ. Press

Williams M, Kothe D, Puckett E. 1998. Accuracy and convergence of continuum surface tension models. In *Fluid Dynamics at Interfaces*, ed. W Shyy, R Narayanan, pp. 294–305. Cambridge, UK: Cambridge Univ. Press

Wroniszewski PA, Verschaeve JC, Pedersen GK. 2014. Benchmarking of Navier–Stokes codes for free surface simulations by means of a solitary wave. *Coast. Eng.* 91:1–17

Xiao F, Ii S, Chen C. 2011. Revisit to the THINC scheme: a simple algebraic VOF algorithm. *J. Comput. Phys.* 230:7086–92

Xu S, Wang ZJ. 2006. An immersed interface method for simulating the interaction of a fluid with moving boundaries. *J. Comput. Phys.* 216:454–93

Young T. 1805. An essay on the cohesion of fluids. *Philos. Trans. R. Soc. Lond.* 95:65–87

Annual Review of Fluid Mechanics

Volume 50, 2018

# Contents

**Indexes**



**Errata**

An online log of corrections to *Annual Review of Fluid Mechanics* articles may be found at http://www.annualreviews.org/errata/fluid